

Supporting Information

Lean-electrolyte lithium–sulfur electrochemical cells with high-loading carbon nanotube/nanofiber–polysulfide cathodes

By Yin-Ju Yen^a and Sheng-Heng Chung^{*,a,b}

Y.-J. Yen, Prof. S.-H. Chung

^aDepartment of Materials Science and Engineering, National Cheng Kung University, No.1,
University Road, Tainan City 701, Taiwan

^bHierarchical Green-Energy Materials Research Center, National Cheng Kung University,
No.1, University Road, Tainan City 701, Taiwan

E-mail: SHChung@gs.ncku.edu.tw

CNT/CNF–polysulfide cathode preparation: The polysulfide catholyte was prepared by mixing 240 mg of sulfur (99.5%, refined, Acros Organics) and 69 mg of lithium sulfide (Li₂S, 99.9%, Acros Organics) in 1 mL of an electrolyte solution, which generated a catholyte containing 1.5 M polysulfide (Li₂S₆), 1.85 M lithium bis(trifluoromethanesulfonyl)imide (LiC₂F₆NS₂O₄ (LITFSI), 99%, Acros Organics), and 0.5 M lithium nitrate (LiNO₃, 99+%, extra pure, Acros Organics) in a mixed 1,2-dimethoxyethane (C₄H₁₀O₂ (DME), 99+%, extra pure, Acros Organics) and 1,3-dioxolane (C₃H₆O₂ (DOL), 99.8%, anhydrous, Acros Organics) solvent with a volume ratio of 50:50. The CNT/CNF composite with a thickness of 50 μm, a weight of 2 mg cm⁻², and a conductivity of 0.05 S sq⁻¹ was a commercial current collector. One CNT/CNF composite was placed at the bottom as the porous current collector. 30 μL of the 1.5 M catholyte was drop-casted on the composite, and then another CNT/CNF composite was placed on the top as the interlayer. The resulting sandwiched CNT/CNF–polysulfide cathode

had a fixed sulfur loading of 8.64 mg cm⁻² and a high sulfur content of 68 wt% considering the total mass of the cathode. This was one of the very few high-loading sulfur cathodes that simultaneously attained high sulfur loading and high sulfur content (Fig. S7 and Table S1).

Materials characterization: The CNT/CNF composite featuring a porous CNT/CNF network with no nanopores was characterized by nitrogen adsorption–desorption analysis and pore-size distribution using an automated gas sorption analyzer (autosorb iQ, Anton Paar) at 77 K with a relative pressure range of 0.00001–1.0. The specific surface area was calculated using the Brunauer–Emmett–Teller adsorption theory, and the nanoporosity was calculated using the Horvath–Kawazoe, density functional theory, and the Barrett–Joyner–Halenda pore size and volume analyses. The morphology, microstructure, and elemental analysis of the CNT/CNF composite and the CNT/CNF–polysulfide cathodes before and after cycling were performed with a scanning electron microscope (SEM, SU-1510, Hitachi) with an energy-dispersive X-ray spectrometer (EDX, XFlash 6|10, BRUKER) for collecting elemental signals and mapping results. The freshly-made CNT/CNF–polysulfide cathodes were retrieved from the assembled lithium–sulfur cells. The cycled lithium–sulfur cells were opened inside an argon-filled glove box to retrieve the cycled CNT/CNF–polysulfide cathodes. Both the freshly-made and cycled CNT/CNF–polysulfide cathodes were rinsed with a mixed DME/DOL solvent and dried in a glove box for the SEM investigation.

Electrochemical characterization: The lithium–sulfur cells were assembled with the CNT/CNF–polysulfide cathode, a polypropylene separator (Celgard), and a lithium-metal foil (Sigma-Aldrich) as the counter electrode. Additional electrolyte was added on the lithium-foil counter electrode to control the low electrolyte-to-sulfur ratios of 4, 5, 6, and 7 $\mu\text{L mg}^{-1}$. The electrolyte was prepared by mixing 1.85 M LiC₂F₆NS₂O₄ (LITFSI) and 0.5 M LiNO₃ in the same mixed DME/DOL solvent, in which the LiNO₃ co-salt creates a passivation film to stabilize the lithium-metal counter electrode and to minor its influences during the electrochemical characterization of our CNT/CNF–polysulfide cathodes. The impedance

spectroscopy data were obtained with a research-grade workstation (SP-150 and VMP-300, Biologic) from 1 MHz to 10 μ Hz with an alternating-current voltage amplitude of 5 mV. The cyclability, Coulombic efficiency, discharge/charge voltage profiles, polarization data, and rate-dependent cyclic voltammetry (CV) data were collected with a programmable battery cycler (BCS-800 series, Biologic) and an electrochemical workstation (VMP-300, Biologic). The cells were first charged to 3.0 V for the initial formation and then discharged and charged between 1.6 and 2.7 V for a full cycle at C/10 and C/5 rates. The current density and the specific capacity were calculated based on the theoretical capacity value and the mass loading of sulfur in the cathode. The areal capacity and energy density values were based on the cathode. The rate-dependent CV analysis was investigated between 1.6 and 2.7 V at scanning rates of 0.02, 0.03, 0.04, and 0.05 mV s^{-1} with each scanning rate (*i.e.*, 0.02, 0.03, 0.04, and 0.05 mV s^{-1}) repeated for three CV scanning cycles. The rate-dependent CV data were collected and examined by the Randles-Sevcik equation:

$$i_{peak} = 268,600 \times e^{1.5} \times area \times coefficient_{Li-ion}^{0.5} \times concentration_{Li-ion} \times rate^{0.5},$$

with i_{peak} as the peak current, e as the number of electrons, $area$ as the cathode area, $coefficient_{Li-ion}$ as the lithium-ion diffusion coefficient, $concentration_{Li-ion}$ as the lithium-ion concentration in the electrolyte, and $rate$ as the scanning rate.

Supporting figures

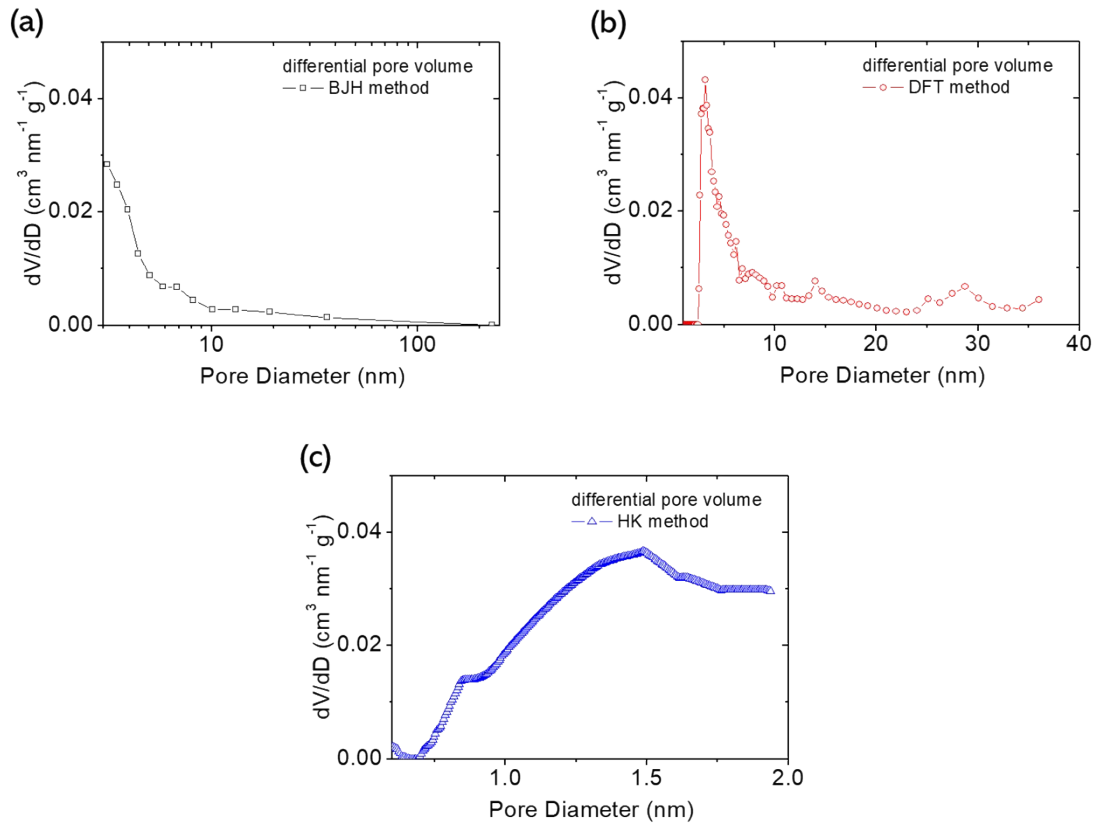


Figure S1. Pore-size distribution analysis of the CNT/CNF composite by: (a) Barrett-Joyner-Halenda (BJH), (b) density functional theory (DFT), and (c) Horvath-Kawazoe (HK) pore size and volume analyses.

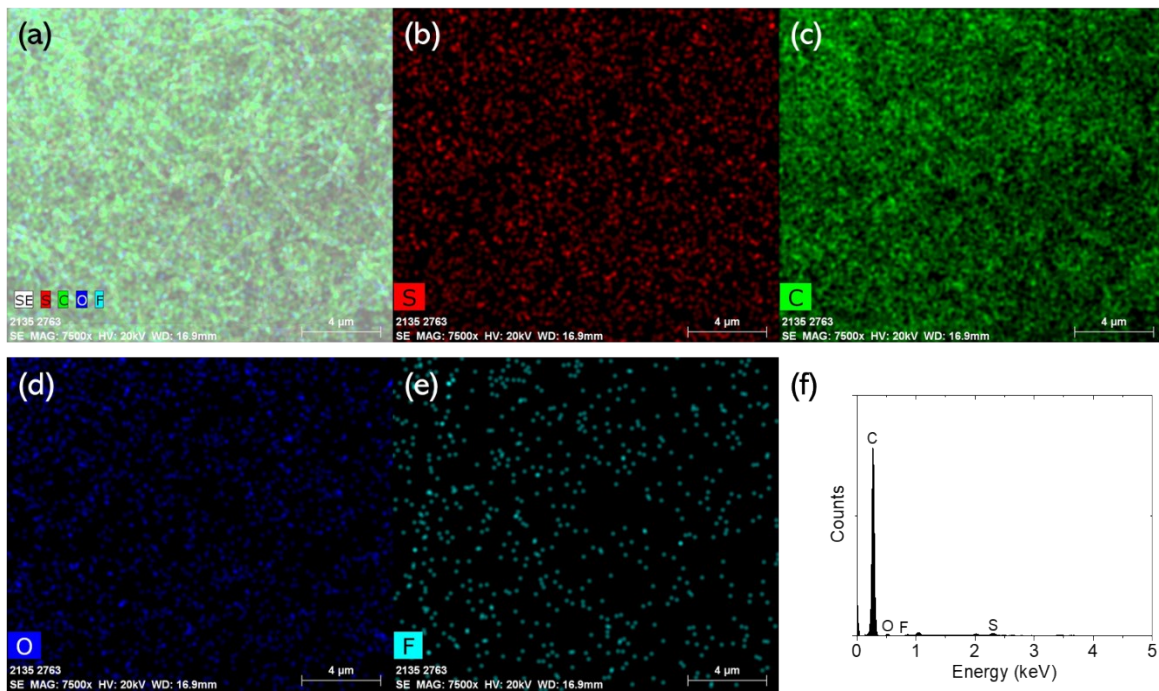


Figure S2. Elemental analysis of the CNT/CNF composite: (a) mapping result with (b) sulfur signals, (c) carbon signals, (d) oxygen signals, (e) fluorine signals, and (f) spectrum.

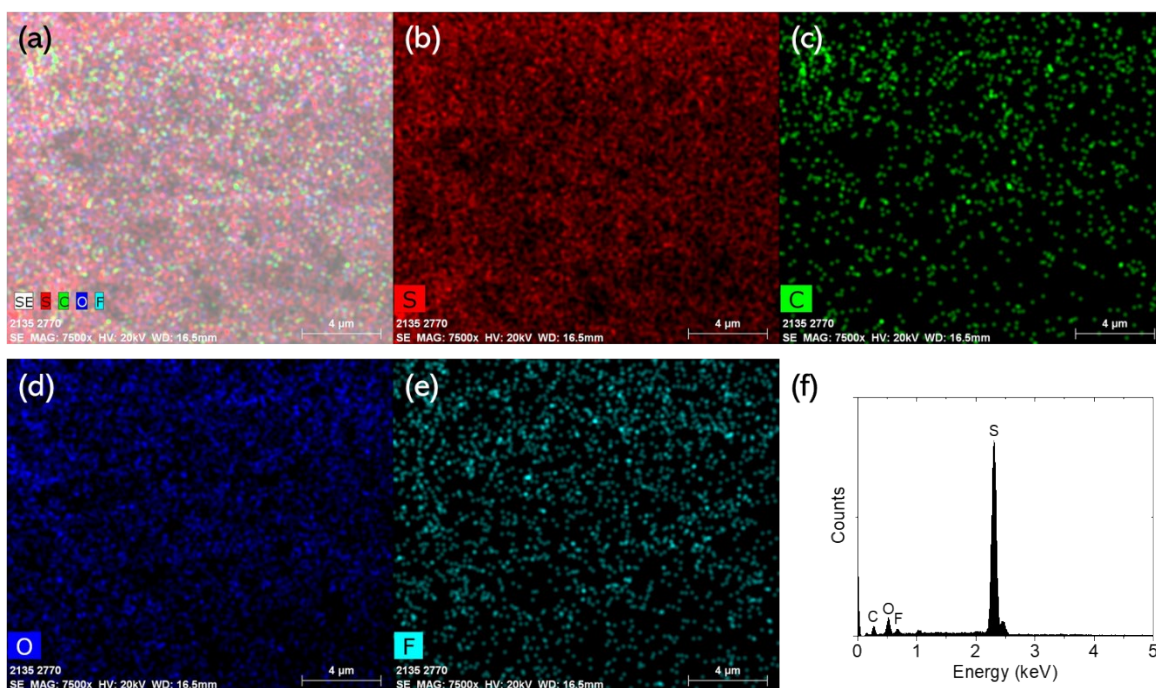


Figure S3. Elemental analysis of the freshly-made CNT/CNF-polysulfide cathode: (a) mapping result with (b) sulfur signals, (c) carbon signals, (d) oxygen signals, (e) fluorine signals, and (f) spectrum.

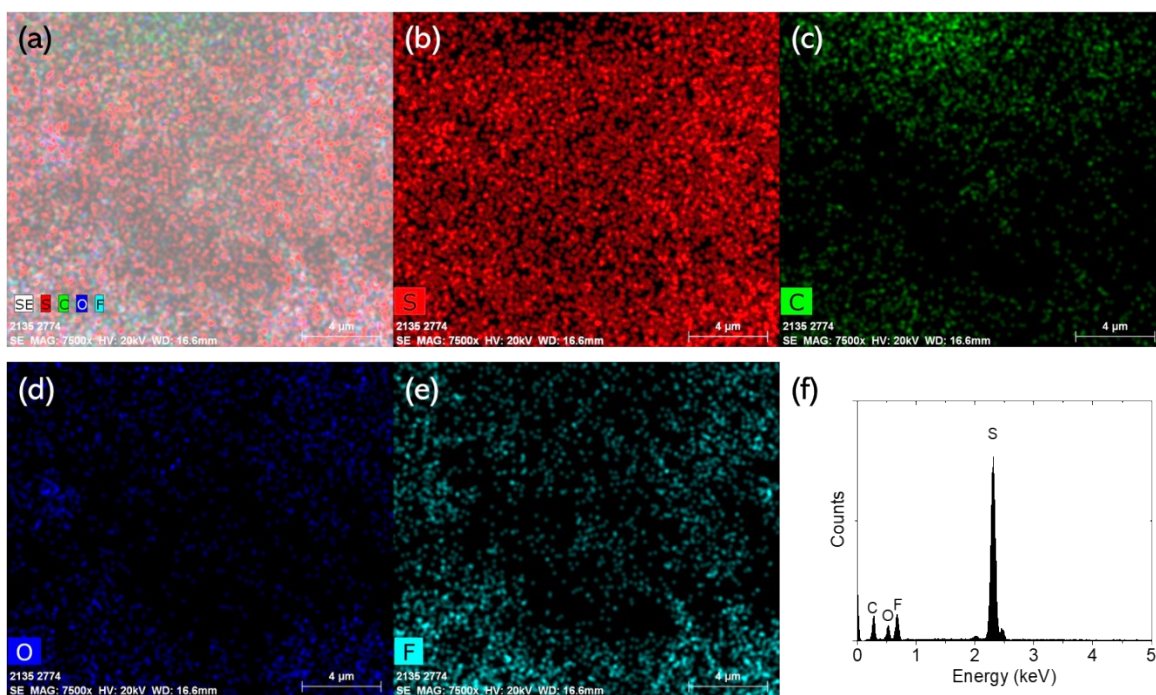


Figure S4. Elemental analysis of the cycled CNT/CNF-polysulfide cathode: (a) mapping result with (b) sulfur signals, (c) carbon signals, (d) oxygen signals, (e) fluorine signals, and (f) spectrum.

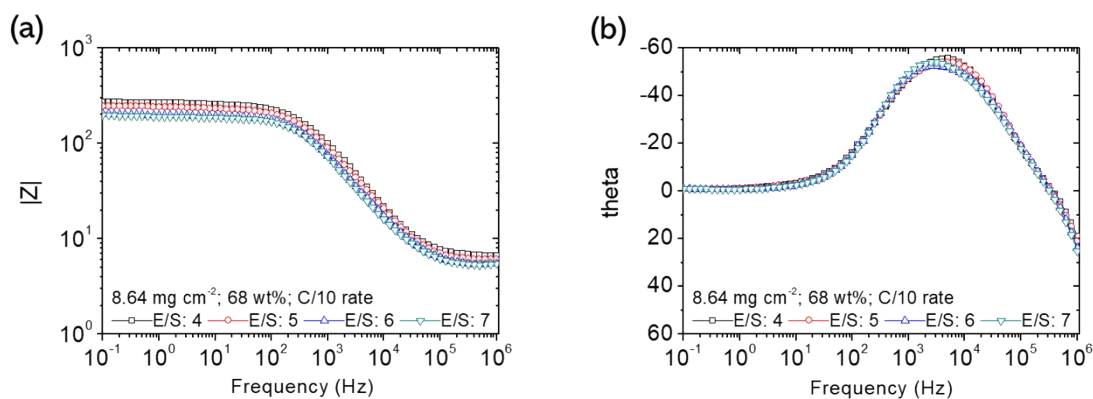


Figure S5. Impedance analysis: Bode plots of the freshly-made CNT/CNF-polysulfide cathode.

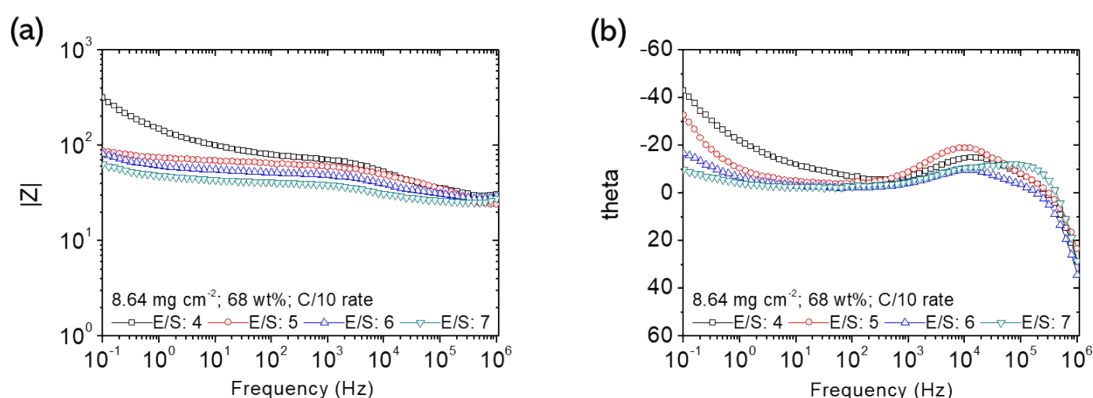


Figure S6. Impedance analysis: Bode plots of the cycled CNT/CNF-polysulfide cathode.

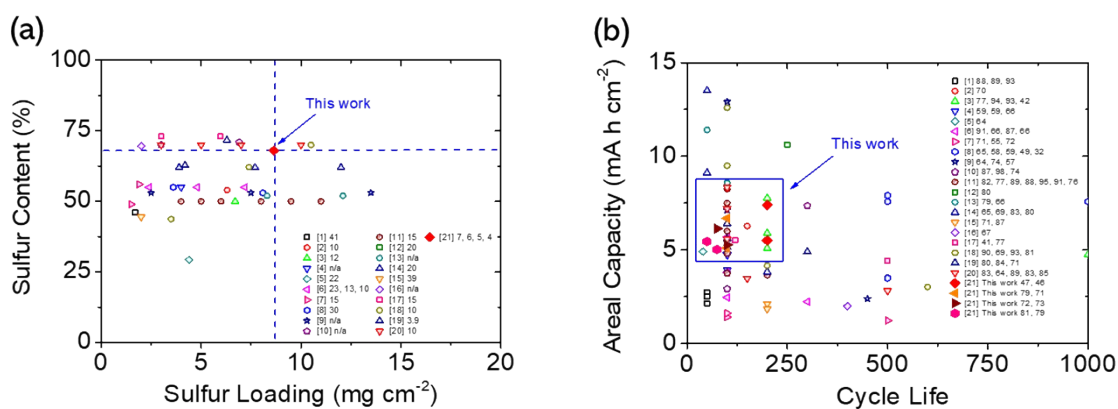


Figure S7. Comparative analysis of the battery performances and electrochemical characteristics of the CNT/CNF-polysulfide cathode with lithium-sulfur researches reporting high sulfur loading, high sulfur content, and/or low electrolyte-to-sulfur ratios: (a) sulfur loading, sulfur content, and electrolyte-to-sulfur ratio (the electrolyte-to-sulfur ratio with an unit as $\mu\text{L mg}^{-1}$ is provided after the number of citations), and (b) areal capacity, cycle life, and capacity retention rate of reported cathodes at lean electrolyte conditions (the capacity retention rate with an unit as % is provided after the number of citations).

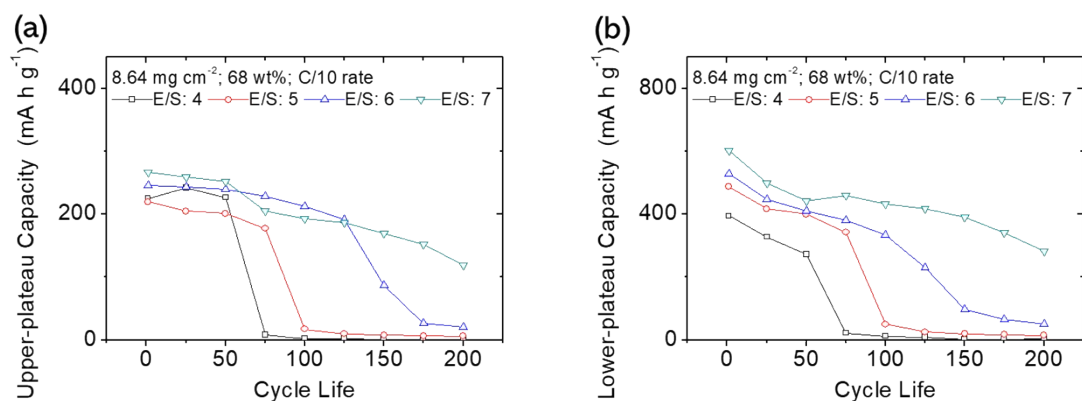


Figure S8. (a) Upper-plateau discharge capacity and (b) lower-plateau discharge capacity analysis of the CNT/CNF-polysulfide cathode at the C/10 rate.

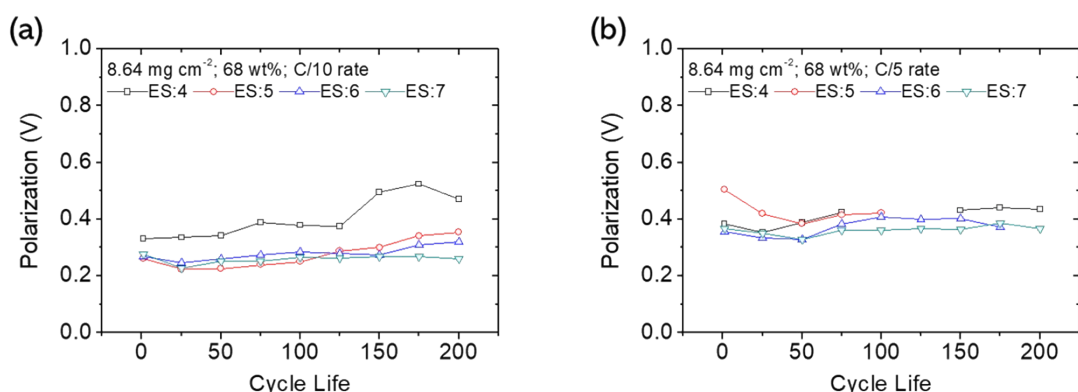


Figure S9. Polarization of the CNT/CNF-polysulfide cathode at (a) C/10 and (b) C/5 rates.

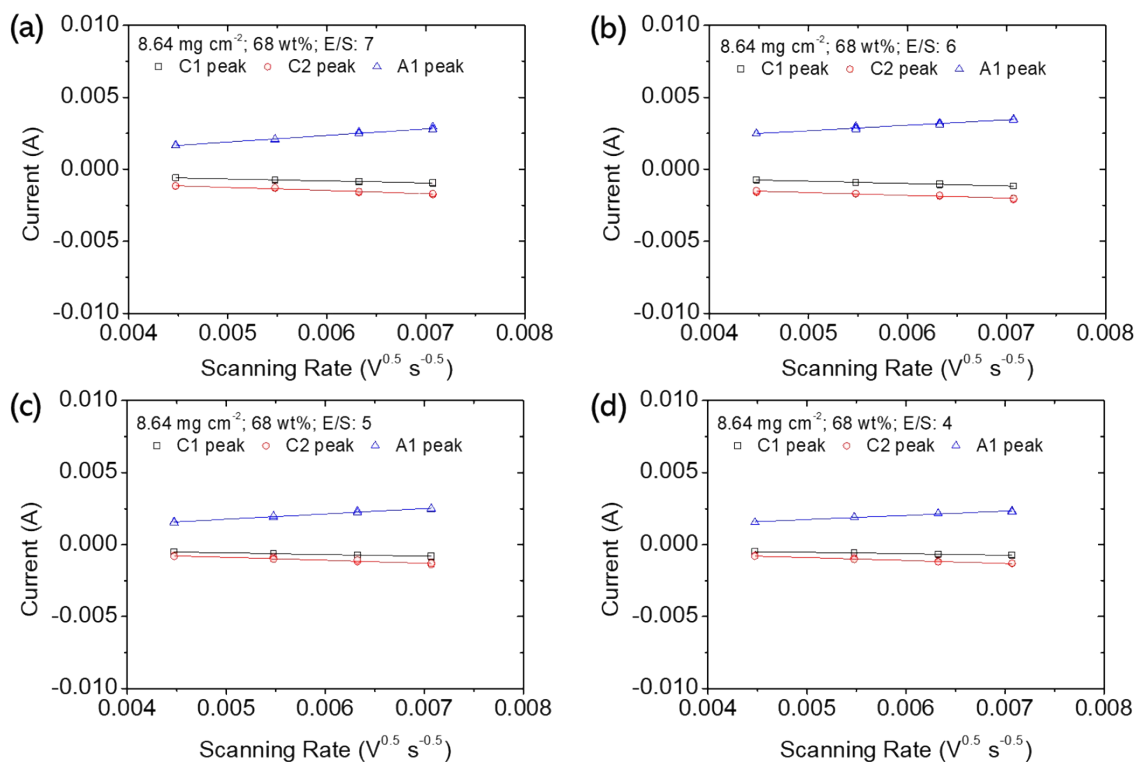


Figure S10. Lithium-ion diffusion coefficient of the CNT/CNF-polysulfide cathode analyzed at 0.02–0.05 mV s^{-1} scanning rates at low electrolyte-to-sulfur ratios of (a) 7, (b) 6, (c) 5, and (d) 4 $\mu\text{L mg}^{-1}$.

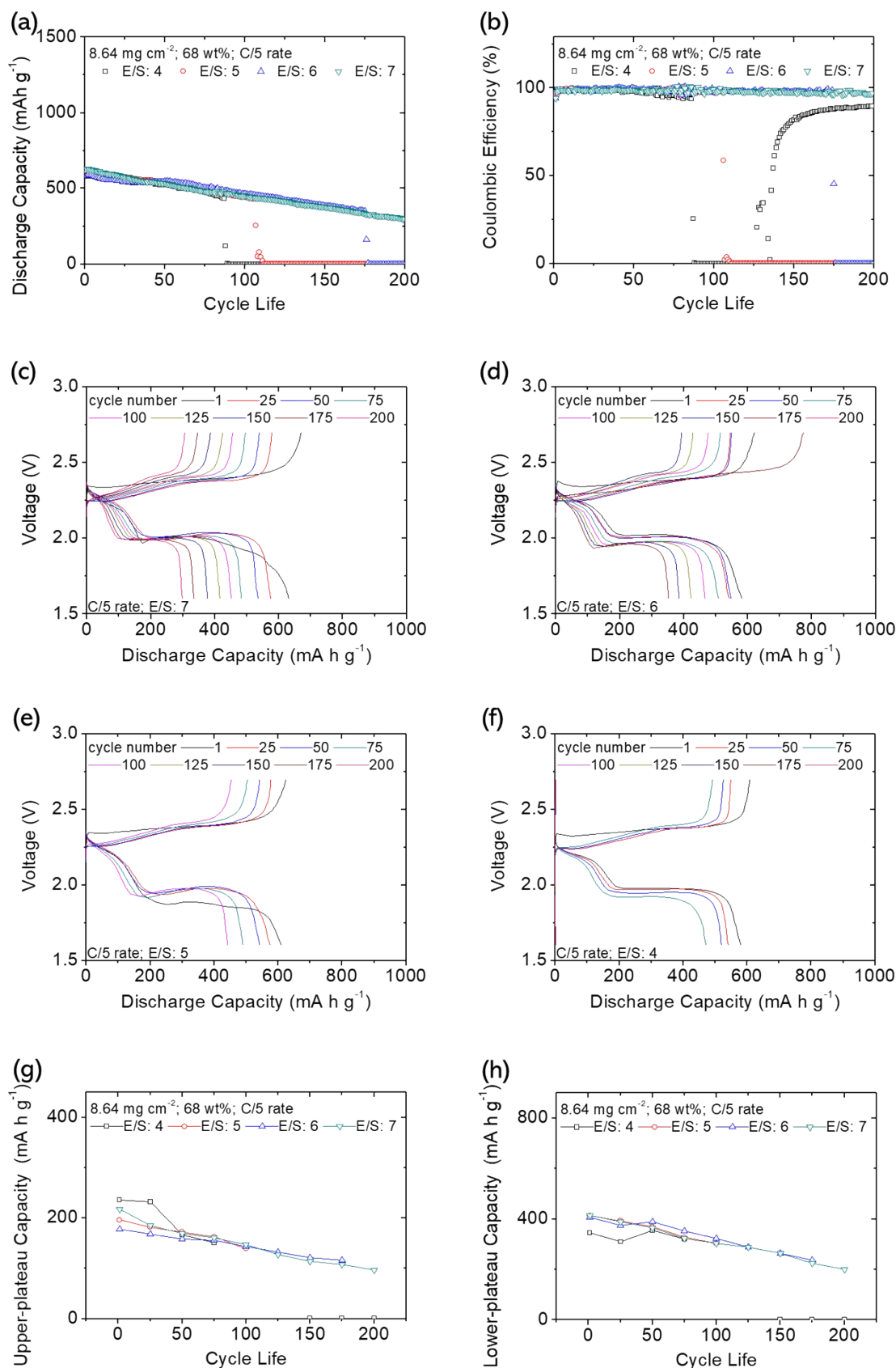


Figure S11. Electrochemical characterization of the CNT/CNF-polysulfide cathode: (a) prolonged cyclability and (b) Coulombic efficiency; discharge/charge voltage profiles at low electrolyte-to-sulfur ratios of (c) 7, (d) 6, (e) 5, and (f) 4 $\mu\text{L mg}^{-1}$; and (g) upper-plateau discharge capacity and (h) lower-plateau discharge capacity analysis at the C/5 rate for 200 cycles.

As a reference and an extended study, Fig. S11 further summarizes the same cell-failure sequence of the CNT/CNF-polysulfide cathode with low E/S ratios of 4–7 $\mu\text{L mg}^{-1}$ during 200 cycles at the fast C/5 rate. Although the CNT/CNF-polysulfide cathode fails to attain 100 cycles at low E/S ratios of 5 and 6 $\mu\text{L mg}^{-1}$ at the C/10 rate, the same cathode completes 100 cycles at the fast C/5 rate (Figs. S11a,S11b). This suggests that a slow cycling rate would be helpful to evaluate the issue of electrolyte consumption in lithium–sulfur batteries. As we investigate the discharge/charge efficiency and the lithiation/delithiation mechanism, Figs. S11c–11f show that the CNT/CNF-polysulfide cathode maintains a stable electrochemical cyclability featuring overlapping discharge and charge curves, whereas Fig. S9b shows similar polarization levels until overcharge occurs at 90, 110, and 175 cycles, which is responsible for the decreased Coulombic efficiency in the cells with E/S ratios of 4, 5, and 6 $\mu\text{L mg}^{-1}$, respectively. The inefficient discharge and charge reactions owing to the decomposition of the catholyte and the consumption of the electrolyte cause the insulating active material to lose its reaction capability, which also decreases the upper-plateau and lower-plateau discharge capacities (Figs. S11g,S11h). However, at a fast cycling rate, the electrochemical conversion of sulfur species has insufficient time to fully complete the conversion steps in each cycle. This incomplete conversion causes slower consumption of the polysulfide catholyte at the faster cycling rate than at a slow cycling rate,^{3,8,9} allowing the CNT/CNF-polysulfide cathode to maintain long-term cycle stability at the fast C/5 rate. According to these findings in the electrochemical analysis, we conclude that CNT/CNF-polysulfide cathode realizes the development of high-loading sulfur cathode at a lean-electrolyte condition and, more importantly, it is necessary to investigate the cyclability at a slow rate and explore the Coulombic efficiency together with the cyclability data to prove the battery performance of lithium–sulfur battery cathodes.

As a result, the electrochemical analysis of the CNT/CNF-polysulfide cathodes (Figs. S11 and 3) might allow us to draw a conclusion on the possible failure mechanism of advanced lithium-sulfur cells with a high-loading sulfur cathode at lean-electrolyte conditions. A high-

loading sulfur cathode reveals the sluggish reaction kinetics of the insulating sulfur, which causes a low electrochemical utilization and reversibility of the cathode.^{4-6,14-17} The further adoption of a lean-electrolyte cell discloses the decrease of the lithium-ion diffusion coefficient and the drying / decomposition of the catholyte.^{6,17-20} The resulting slow lithium-ion transfer and fast consumption of the electrolyte would damage the inner ion transfers and exacerbate the insulating precipitation on the cathode, eventually leading to the cell failure featuring the unstable discharge/charge efficiency, followed by the decrease of electrochemical reversibility and utilization of the active material.¹⁴⁻¹⁷ Thus, it is instructive to study the Coulombic efficiency and slow-rate testing to complete the evaluation of the designed high-loading sulfur cathodes at lean electrolyte conditions.

Accordingly, an investigation of the failure mechanism of the CNT/CNF-polysulfide cathode reveals a probable cell-failure sequence in which overcharge occurs as a result of the rapid consumption of electrolyte due to the low E/S ratio, leading to slow ion diffusion, decreased Coulombic efficiency, and irreversible capacity loss. Therefore, the development of high-loading CNT/CNF-polysulfide cathodes at a lean-electrolyte condition and the investigation of their failure mechanism further suggest the importance of studying the slow-rate and Coulombic-efficiency performances together with the cyclability data to ensure the electrochemical efficiency and reversibility of lithium-sulfur battery cathodes.

Supporting tables

Table S1. Comparative analysis of the battery performances and electrochemical characteristics of the CNT/CNF-polysulfide cathode with lithium-sulfur researches reporting high sulfur loading, high sulfur content, and/or low electrolyte-to-sulfur ratios.

Year	Sulfur loading (mg cm ⁻²)	Sulfur content (wt%)	Electrolyte-to-sulfur ratio (μL mg ⁻¹)	Cycling rate	Cycle life	Highest capacity (mA·h g ⁻¹)	Areal capacity (mA·h cm ⁻²)	Ref.
2013	1.7	46	41	C/10	50	1,600	2.72	S1
				C/5	50	1,469	2.50	S1
				C/2	50	1,261	2.14	S1
2014	6.3	54	10	C/20	150	995	6.27	S2
2015	6.7	50	12	C/5	200	1,160	7.77	S3
				C/2	200	880	5.90	S3
				1C	200	760	5.09	S3
				1.5C	1000	709	4.75	S3
2015	4	55	n/a	C/10	100	1,190	4.76	S4
				C/5	100	1,180	4.72	S4
				C/3	100	980	3.92	S4
2016	4.4	29.3	22	C/20	40	1,116	4.91	S5
2016	2.4	55	23	C/5	100	1,022	2.45	S6
	2.4	55	23	C/2	300	930	2.23	S6
	4.8	55	13	C/2	100	790	3.79	S6
	7.2	55	10	C/2	100	790	5.69	S6
2017	1.5	49	15	C/4	100	961	1.41	S7
	1.5	49	15	1C	500	830	1.22	S7
	1.9	56	15	C/4	100	825	1.61	S7
2017	3.6	55	30	C/4	500	974.2	3.51	S8
	3.6	55	30	C/2	500	968.3	3.49	S8
	8.1	53	30	C/4	500	976.4	7.91	S8
	8.1	53	30	C/2	500	935.6	7.58	S8
	8.1	53	30	C/2	1000	935.6	7.58	S8

2017	2.5	53	n/a	1C	450	953	2.38	S9
	7.5	53	n/a	C/3	100	950	7.13	S9
	13.5	53	n/a	C/3	100	957	12.92	S9
2017	3	70	n/a	C/5	100	1,258.8	3.78	S10
	3	70	n/a	1C	100	973	2.92	S10
	6.9	71	n/a	C/5	300	1,067	7.36	S10
2018	4	50	15	C/10	100	938	3.75	S11
	5	50	15	C/2	200	728	3.64	S11
	6	50	15	C/10	100	875	5.25	S11
	6	50	15	C/5	100	800	4.80	S11
	8	50	15	C/5	100	750	6.00	S11
	9.5	50	15	C/5	100	789	7.50	S11
	11	50	15	C/10	100	750	8.25	S11
2018	8.1	60	20	C/10	250	1,310.8	10.62	S12
2018	8.3	52	n/a	C/5	100	1,033	8.57	S13
	12.1	52	n/a	C/2	50	943	11.41	S13
2018	3.9	62	20	C/10	100	1,321.7	5.15	S14
	3.9	62	20	C/2	200	980	3.82	S14
	7.7	62	20	C/10	50	1,183.7	9.11	S14
	12	62	20	C/10	50	1,125.8	13.51	S14
2019	2	44	39	C/2	200	1,060	2.21	S15
	2	44	39	1C	200	920	1.84	S15
2019	2	69.6	n/a	C/5	400	997	1.99	S16
2020	3	73	15	C/2	500	1,473	4.42	S17
	5.98	73	15	1C	120	923	5.52	S17
2020	3.5	44	10	C/2	200	1,188	4.16	S18
	3.5	44	10	1C	600	862	3.02	S18
	7.4	62	10	C/10	100	1,284	9.50	S18
	10.5	70	10	C/10	100	1,200	12.60	S18

2020	4.19	63	3.9	C/5	300	1,166	4.89	S19
	6.29	72	3.9	C/5	100	1,017	6.40	S19
	6.29	72	3.9	C/2	100	890	5.60	S19
2020	3	70	10	C/5	150	1,157	3.47	S20
	3	70	10	1C	500	937	2.81	S20
	5	70	10	C/5	100	1,116	5.58	S20
	7	70	10	C/5	100	1,030	7.21	S20
	10	70	10	C/5	100	834	8.34	S20
2020	8.64	68.4	7	C/5	200	631	5.45	This work
	8.64	68.4	7	C/10	200	870	7.52	This work
	8.64	68.4	6	C/5	100	590	5.10	This work
	8.64	68.4	6	C/10	100	774	6.69	This work
	8.64	68.4	5	C/5	100	610	5.27	This work
	8.64	68.4	5	C/10	75	710	6.13	This work
	8.64	68.4	4	C/5	75	581	5.02	This work
	8.64	68.4	4	C/10	50	630	5.44	This work

Table S2. Lithium-ion diffusion coefficient of the lean-electrolyte cell with the CNT/CNF-polysulfide cathode.

Electrolyte-to-sulfur ratio	Lithium-ion diffusion coefficient (C1) ($\text{cm}^2 \text{s}^{-1}$)	Lithium-ion diffusion coefficient (C2) ($\text{cm}^2 \text{s}^{-1}$)	Lithium-ion diffusion coefficient (A1) ($\text{cm}^2 \text{s}^{-1}$)
7	1.0×10^{-8}	2.5×10^{-8}	1.1×10^{-7}
6	1.3×10^{-8}	2.3×10^{-8}	7.2×10^{-8}
5	6.5×10^{-9}	2.1×10^{-8}	6.9×10^{-8}
4	4.7×10^{-9}	2.0×10^{-8}	4.3×10^{-8}

Supporting references

- S1 Y. Fu, Y.-S. Su, and A. Manthiram, *Angew. Chem. Int. Ed.*, 2013, **52**, 6930-6935.
- S2 Z. Yuan, H. J. Peng, J. Q. Huang, X. Y. Liu, D. W. Wang, X. B. Cheng and Q. Zhang, *Adv. Funct. Mater.* 2014, **24**, 6105–6112.
- S3 J. Yan, X. Liu, H. Qi, W. Li, Y. Zhou, M. Yao and B. Li, *Chem. Mater.* 2015, **27**, 6394–6401.
- S4 X. Yu, Z. Bi, F. Zhao and A. Manthiram, *ACS Appl. Mater. Interfaces* 2015, **7**, 16625–16631.
- S5 S. Waluś, C. Barchasz, R. Bouchet, J. F. Martin, J. C. Leprêtre and F. Alloin, *Electrochim. Acta* 2016, **211**, 697–703.
- S6 H. Xu, L. Qie and A. Manthiram, *Nano Energy* 2019, **26**, 224-232.
- S7 S. Han, X. Pu, X. Li, M. Liu, M. Li, N. Feng, S. Dou and W. Hu, *Electrochim. Acta* 2017, **241**, 406-413.
- S8 M. Yu, J. Ma, M. Xie, H. Song, F. Tian, S. Xu, Y. Zhou, B. Li, D. Wu, H. Qiu and R. Wang, *Adv. Energy Mater.* 2017, **7**, 1602347.
- S9 H. Xu and A. Manthiram, *Nano Energy* 2017, **33**, 124-129.
- S10 Y. Liu, G. Li, Z. Chen and X. Peng, *J. Mater. Chem. A* 2017, **5**, 9775–9784.
- S11 X. Chen, L. Yuan, Z. Hao, X. Liu, J. Xiang, Z. Zhang, Y. Huang and J. Xie, *ACS Appl. Mater. Interfaces* 2018, **10**, 13406–13412.
- S12 Y. Zhong, D. Chao, S. Deng, J. Zhan, R. Fang, Y. Xia, Y. Wang, X. Wang, X. Xia and J. Tu, *Adv. Funct. Mater.* 2018, **28**, 1706391.
- S13 X. Zhao, M. Kim, Y. Liu, H. J. Ahn, K. W. Kim, K. K. Cho, and J. H. Ahn, *Carbon* 2018, **128**, 138-146.
- S14 Y. Z. Zhang, Z. Zhang, S. Liu, G. R. Li and X. P. Gao, *ACS Appl. Mater. Interfaces* 2018, **10**, 8749–8757.
- S15 Q. Lu, Y. Sun, K. Liao, X. Zou, I. Hamada, W. Zhou, M. Ni and Z. Shao, *Electrochim.*

- Acta* 2019, **298**, 421-429.
- S16 J. Kim, Y. Kang, S. W. Song and J. Suk, *Electrochim. Acta* 2019, **299**, 27-33.
- S17 H. Li, D. Liu, X. Zhu, D. Qu, Z. Xie, J. Li, H. Tang, D. Zheng and D. Qu, *Nano Energy* 2020, **73**, 104763.
- S18 S. Niu, S. W. Zhang, R. Shi, J. Wang, W. Wang, X. Chen, Z. Zhang, J. Miao, A. Amini, Y. Zhao and C. Cheng, *Energy Storage Mater.* 2020, **33**, 73–81.
- S19 S. Yao, R. Guo, F. Xie, Z. Wu, K. Gao, C. Zhang, X. Shen, T. Li and S. Qin, *Electrochim Acta* 2020, **337**, 135765.
- S20 L. Luo, J. Li, H. Yaghoobnejad Asl and A. Manthiram, *ACS Energy Lett.* 2020, **5**, 1177–1185.